CHAPTER 3

RESULTS AND DISCUSSION

3. 1 Result of the products synthesized by a hydrothermal method using ammonium metatungstate hydrate as a tungsten source

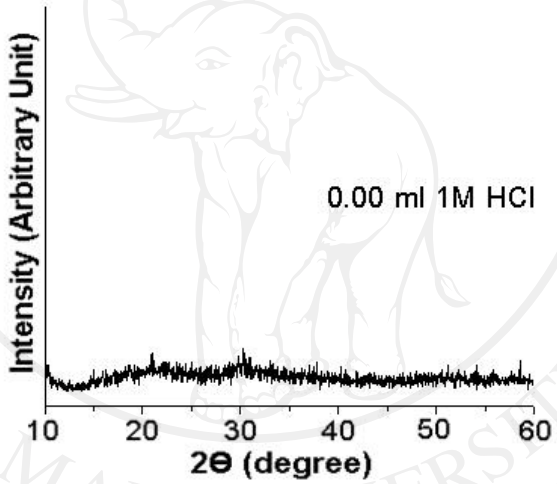

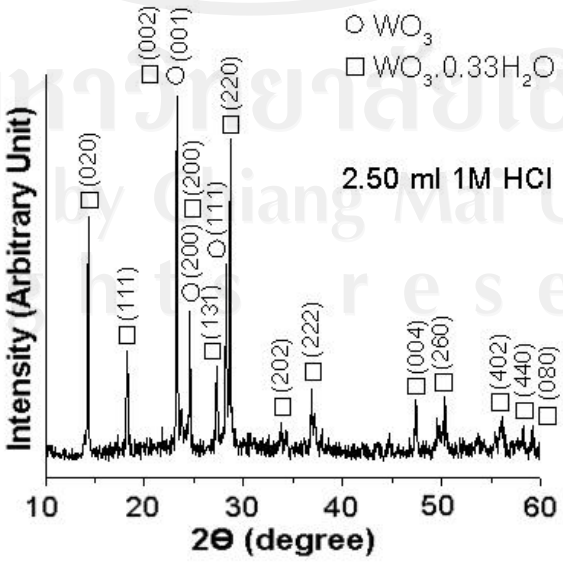

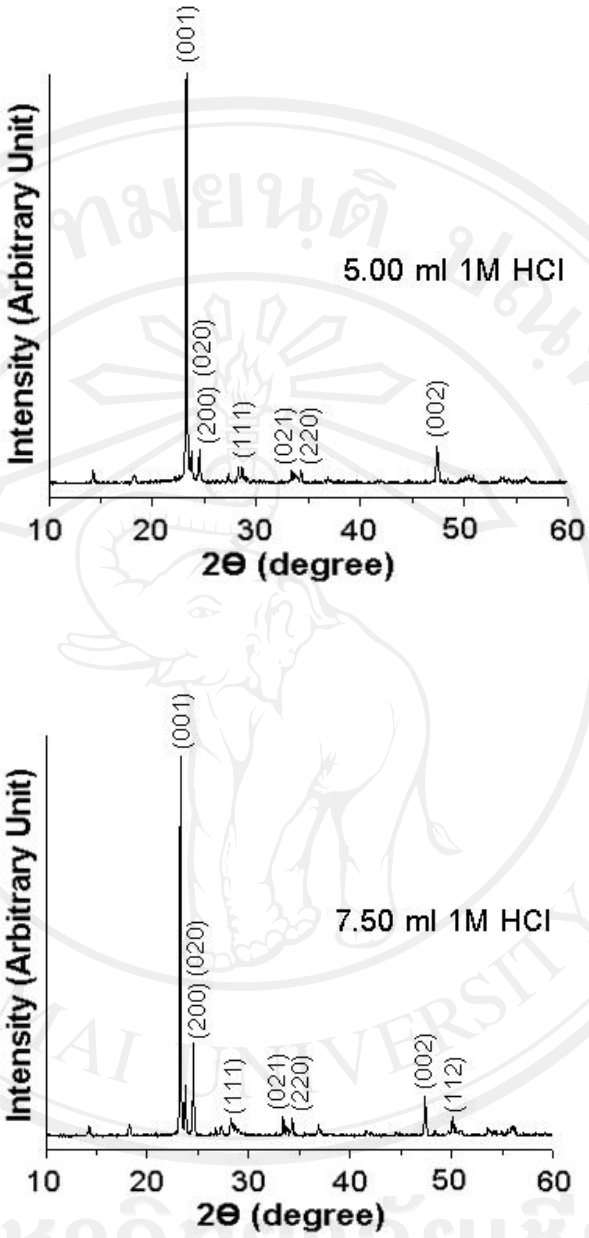

Figure 3.1 XRD patterns of the products synthesized by the hydrothermal reaction at 200 °C for 24 h in the solutions containing 0.00, 2.50 ml, 5.00 ml, and 7.50 ml of 1M HCl.

Figure 3.1 shows the XRD patterns of the products synthesized by 200 °C, 24 h hydrothermal reactions using ammonium metatungstate hydrate and CTAB as a tungsten source and surfactant, with 0–7.50 ml 1M HCl added. In the HCl-free solution, the product was an amorphous phase. When 2.50 ml 1M HCl was added to the solution, both orthorhombic $WO_3 \cdot 0.33H_2O$ (JCPDS No. 35-0270) and WO_3 phases (JCPDS No. 20-1324) [29] were detected. These products became pure orthorhombic WO_3 (o-WO_3) in the 5.00 ml and 7.50 ml 1M HCl-added precursor solutions. The analysis implies that HCl has an influence on the synthesis of pure o-WO_3 phase.

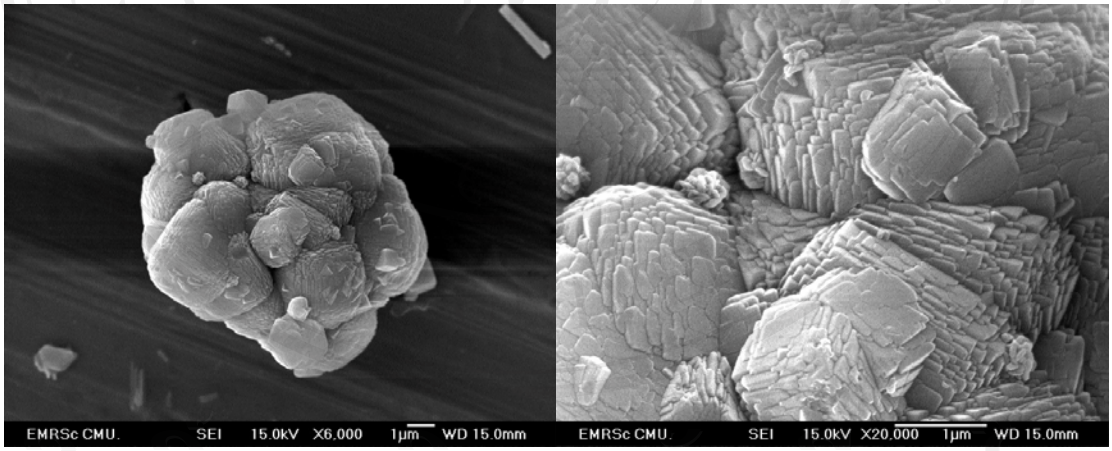

Figure 3.2 SEM images at low and high magnifications of the product synthesized by the hydrothermal reaction at 200 °C for 24 h in the solution containing 5.00 ml of 1M HCl.

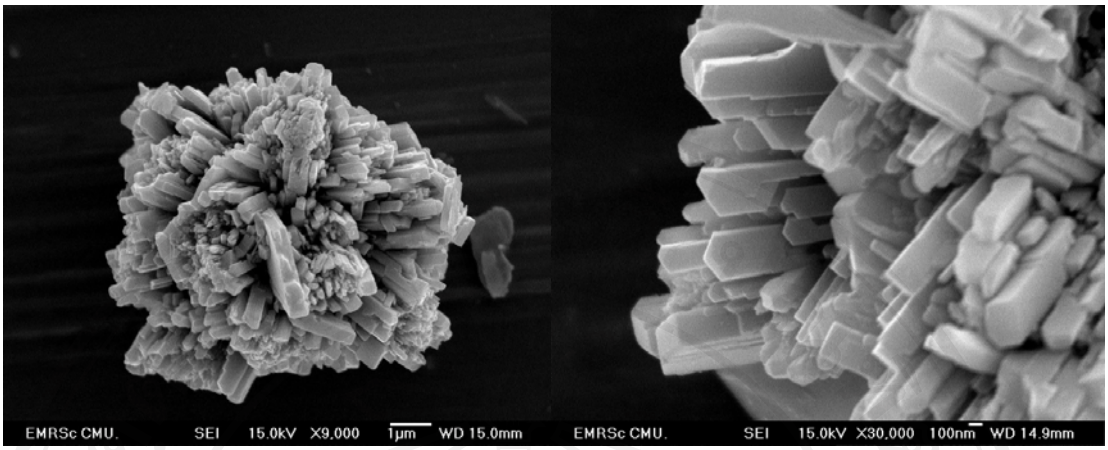

Figure 3.3 SEM images at low and high magnifications of the product synthesized by the hydrothermal reaction at 200 °C for 24 h in the solution containing 7.50 ml of 1M HCl.

SEM images (Figure 3.2) show o-WO_3 in the shape of ~8 μm microseeds in numerous square layers in the 5.00 ml 1M HCl-added solution. By increasing 1M HCl from 5.00 ml to7.50 ml, these microsquare layers grew out of the microseed cores to form microflower-like particles (Figure 3.3), composed of 2–3 μm×100–300 nm×100–300 nm petals with very smooth surfaces.

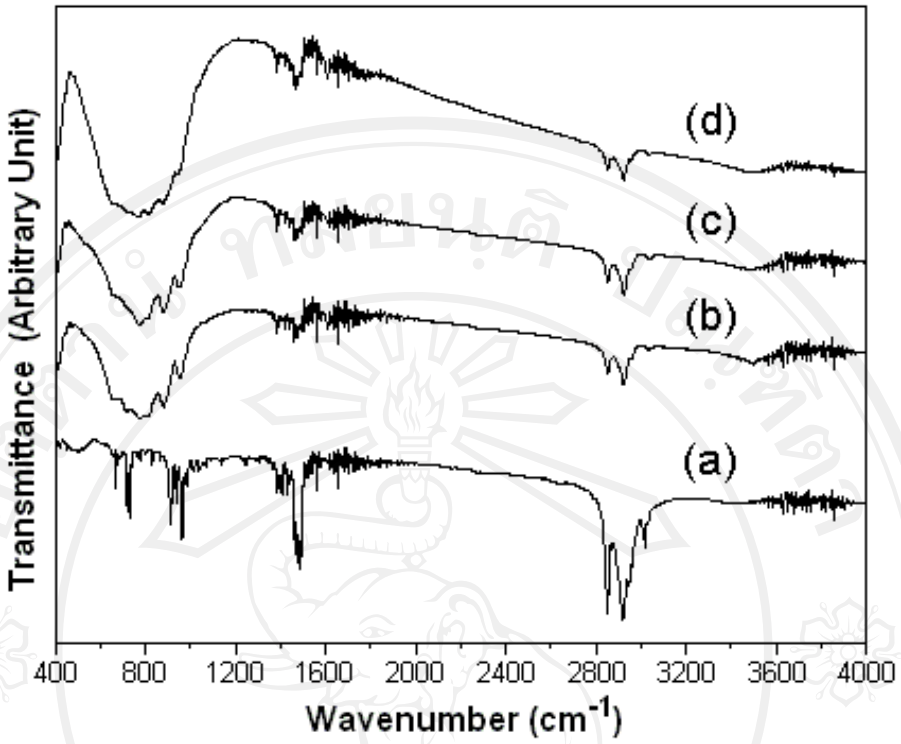

Figure 3.4 FTIR spectra of (a) CTAB, and (b–d) the products synthesized by the hydrothermal reaction at 200 °C for 24 h in the solutions containing 2.50 ml, 5.00 ml, and 7.50 ml of 1M HCl, respectively.

The products were further characterized by FTIR spectroscopy in the range of 400–4000 cm^{-1}, and the vibrations compared to those of CTAB. Some bands were detected at 2800–3020 cm^{-1}, which can be attributed to the CTAB surfactant. The FTIR spectrum of CTAB shows two intense bands at 2918 and 2846 cm^{-1}, corresponding to the asymmetric and symmetric stretching vibrations of $C–CH_2$ in the methylene chains. The sharp bands at 1450–1500 cm^{-1} were specified as the deformation of $–CH_2–$ and $–CH_3$, and the weak band at 3011 cm^{-1} as the $C–CH_3$ asymmetric stretching and $N–CH_3$ symmetric stretching vibrations of the solid

surfactant [30–33]. In case of the as-synthesized products, broad bands between 590 and 949 cm^{-1} were detected. They are attributed to the stretching of short W=O bonds, while the bands at 817 and 728 cm^{-1} were assigned to be the O–W–O stretching modes. The vibrational bands centered at 659 and 590 cm^{-1} were attributed to the W–O–W stretching modes [11]. The asymmetric and symmetric stretching vibrations of CH_2 in the methylene chains of the incorporated CTAB were also detected at the same wavenumbers as those of the solid surfactant – implying that no intermolecular interaction was enhanced due to the capping effect, and the conformation of methylene chains remained unchanged. Their intensities are weakened, because CTAB was not completely removed by washing with deionized water and ethanol, and remained as the adsorbed head groups on the surfaces of these products – as was also found in previous reports [30, 31, 33].

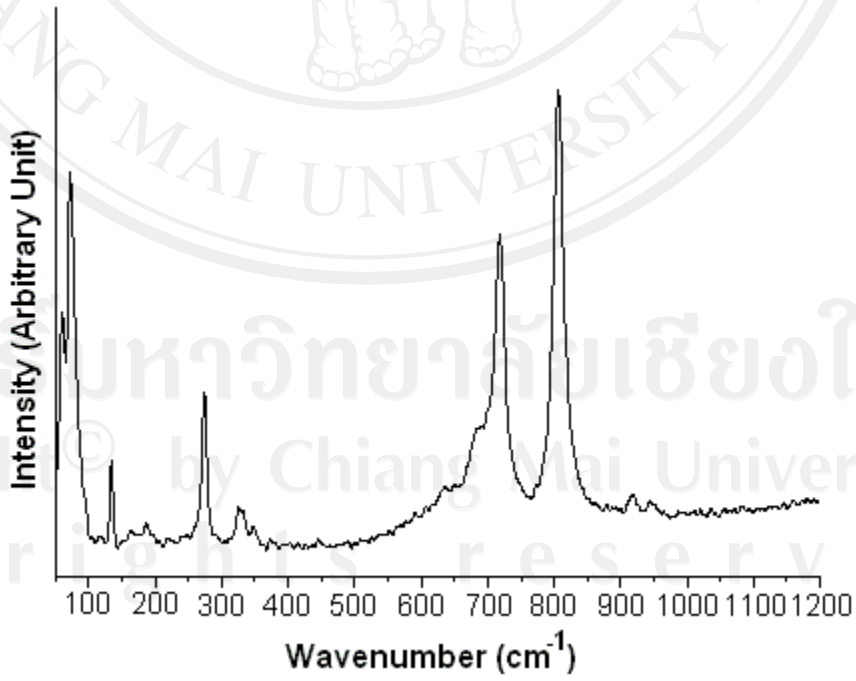

Figure 3.5 Raman spectrum of o-WO_3 microflowers, synthesized by the hydrothermal reaction at 200 °C for 24 h in the solution containing 7.50 ml 1M HCl.

The Raman spectrum of the as-synthesized WO_3 microflowers over the range of 50–1200 cm^{-1} is shown in Figure 3.5. The Raman spectrum detected vibrational peaks at 806, 718, 686, 326, 274, 134, 76 and 60 cm^{-1}. The two main intense peaks at 806 and 718 cm^{-1}, and the shoulder at 686 cm^{-1}, are typical Raman peaks of crystalline WO_3, which correspond to the stretching and bending vibrations of the bridging tungsten and oxygen atoms. They are assigned to be the W–O stretching (ν), W–O bending (δ) and O–W–O deformation (γ) modes, respectively. Two peaks at 326 and 274 cm^{-1} are assigned to be the bending δ (O–W–O) vibrations. Those below 200 cm^{-1} modes were attributed to the lattice vibrations. All these peaks are in good accordance with those of other reports [11, 25, 34-36].

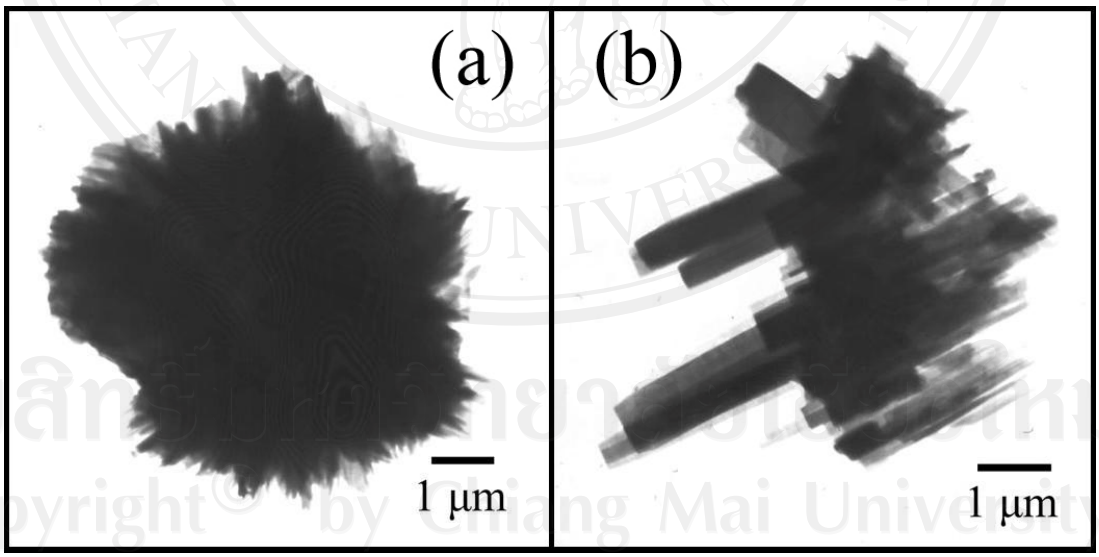

Figure 3.6 TEM images of o-WO_3 microflowers, synthesized by the hydrothermal reaction at 200 °C for 24 h in the solution containing 7.50 ml 1M HCl.

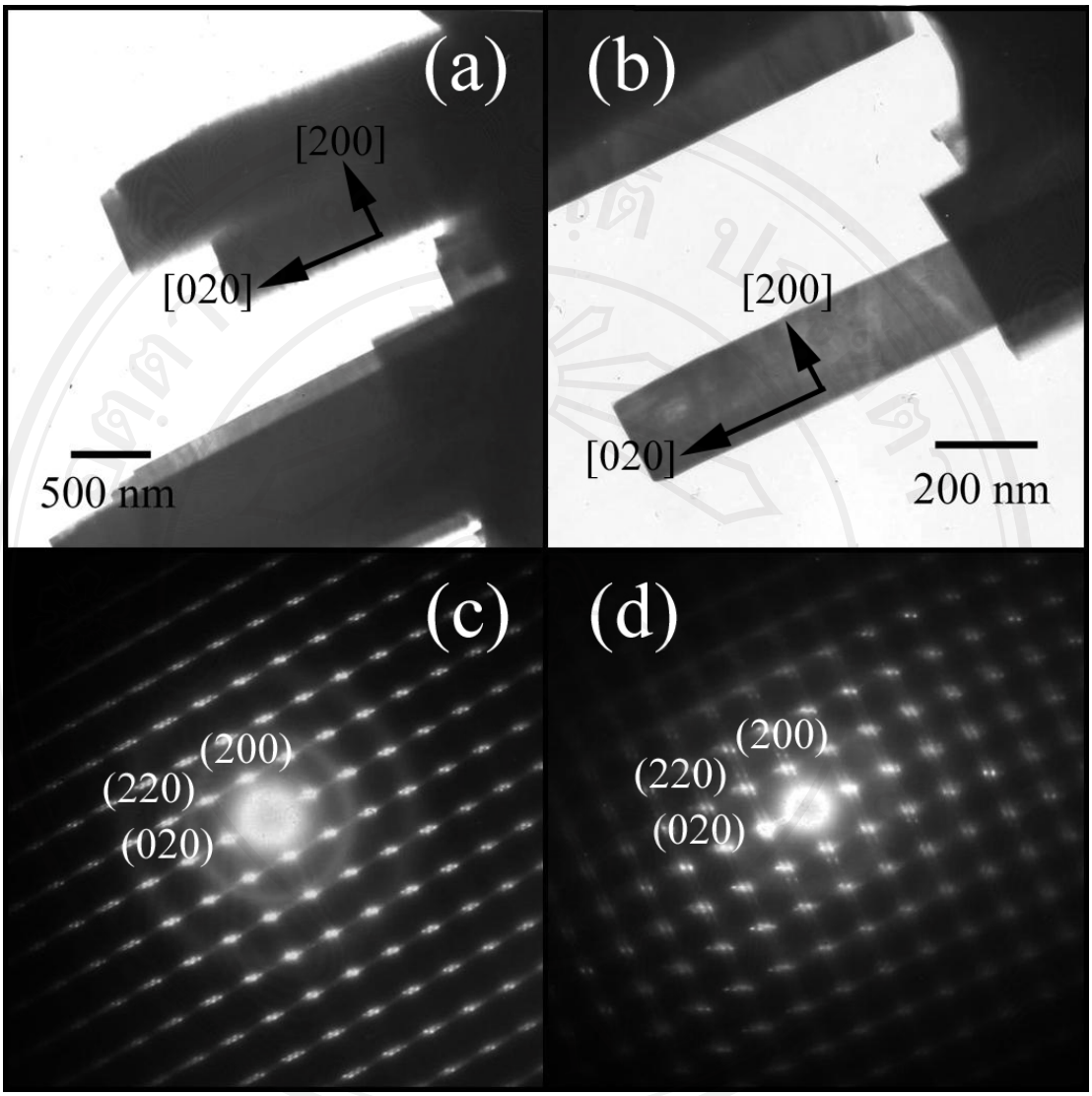

Figure 3.7 (a, b) High magnification TEM images, and (c, d) SAED patterns of o-WO_3 microflowers of Figure 3.6 (b).

Detailed morphology of the as-synthesized o-WO_3 structure was proved by TEM images (Figure 3.6), which show the product shape to be microflowers 6–8 μm in diameter; these are composed of a large number of petals with lengths up to several micrometers. Some petals were released from the microflowers cores by ultrasonic

vibrations during preparation of the samples for TEM analysis. Figure 3.7 (a and b) presents high-magnification TEM images with the x-axis of Figure 3.6 (b) tilted. These o-WO_3 petals are straight and smooth, with uniform dimension along their axial direction. The selected area electron diffraction patterns (Figure 3.7 (c and d)) were indexed and specified as orthorhombic WO_3 phase (JCPDS No. 20-1324) [29], in accordance with the XRD analysis. They show the (0 2 0), (2 2 0) and (2 0 0) diffraction planes with the electron beam in the [0 0−1] direction. It should be noted that the growth direction of the petals is normal to the (0 2 0) plane of the microsquare layers – implying that the o-WO_3 microsquare layers are aligned along the [0 2 0] direction.

The formation of o-WO_3 microflowers can be explained by polycondensation, electroneutral and dehydration reactions from the polyoxotungstate anions, as shown below:

$$H_2W_{12}O_{40}^{6-} + 6H^+ + (8 + n)H_2O \rightarrow 12H_2WO_4.nH_2O \quad (1)$$

$$H_2WO_4.nH_2O \rightarrow o\text{-}WO_3(\text{nuclei}) + (n + 1)H_2O \quad (2)$$

$$o\text{-}WO_3(\text{nuclei}) \rightarrow WO_3(\text{microflowers}) \quad (3)$$

When $(NH_4)_6H_2W_{12}O_{40}{\cdot}xH_2O$ was dissolved in deionized water, followed by the addition of HCl, the colorless solution of $H_2W_{12}O_{40}^{6-}$ anions changed to $H_2WO_4.nH_2O$ yellow precursor precipitates. Upon the 200 ◦C hydrothermal reaction, $H_2WO_4.nH_2O$ was further decomposed to produce o-WO_3 (nuclei) [37–39], containing in microsquare layers of $[WO_6]^{6-}$ octahedrons [11, 35] lying in the [2 0 0] direction. At this stage, CTAB – which is a positively charged cationic surfactant (CTA^+) with a long hydrophobic tail [30, 40, 41] – was attracted by the four

negatively charged oxygen atoms in the planar surface of $[WO_6]^{6-}$, due to the stereochemical effect. The $[CTA–WO_6]^{2-}$ bonds orientated parallel to the [0 2 0] direction inhibited growth in the [2 0 0] and [0 0 2] directions because of the CTA^+ hydrophobic tails [38, 40]. The $[CTA–WO_6]^{2-}$ petals grew out from cores to form o-WO_3 microflowers, and the CTAB molecules were washed out, as shown in Figure 3.8

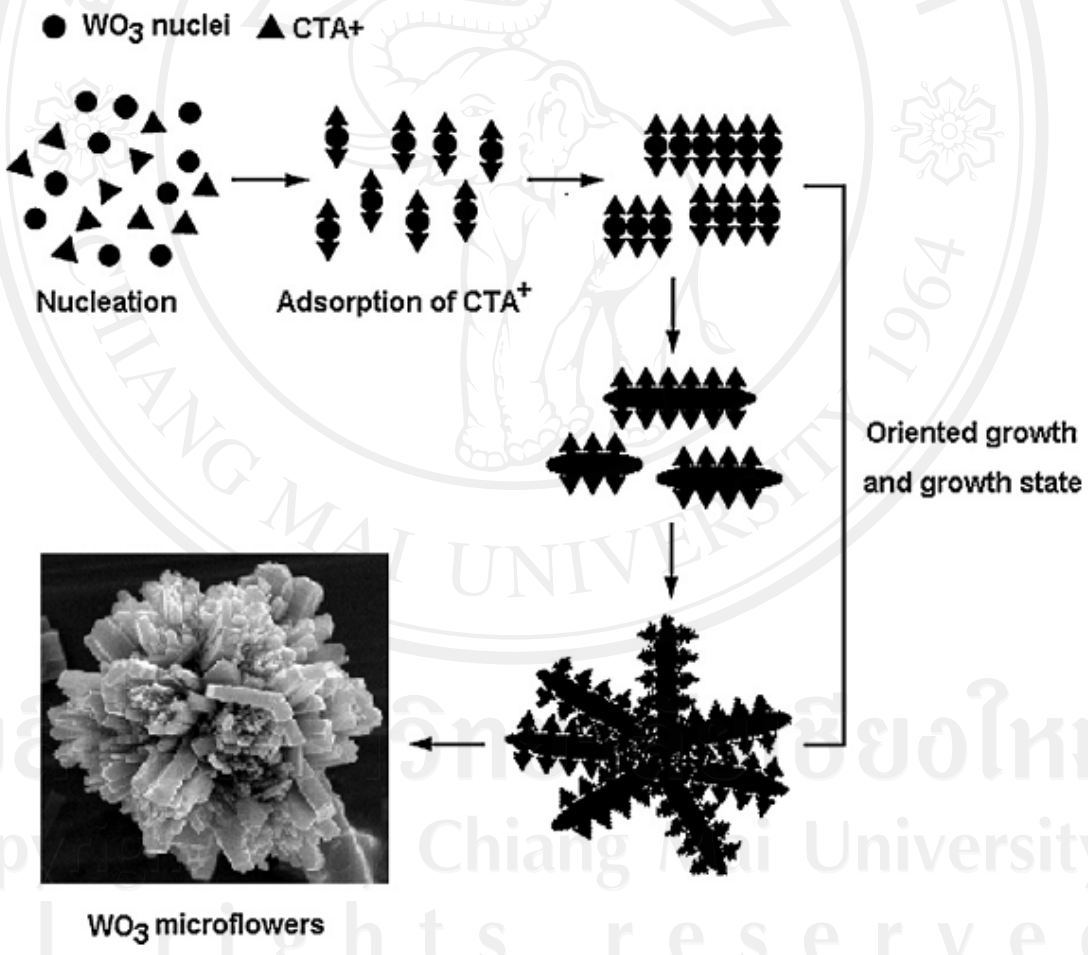

Figure 3.8 Schematic diagram for the formation of o-WO_3 microflowers.

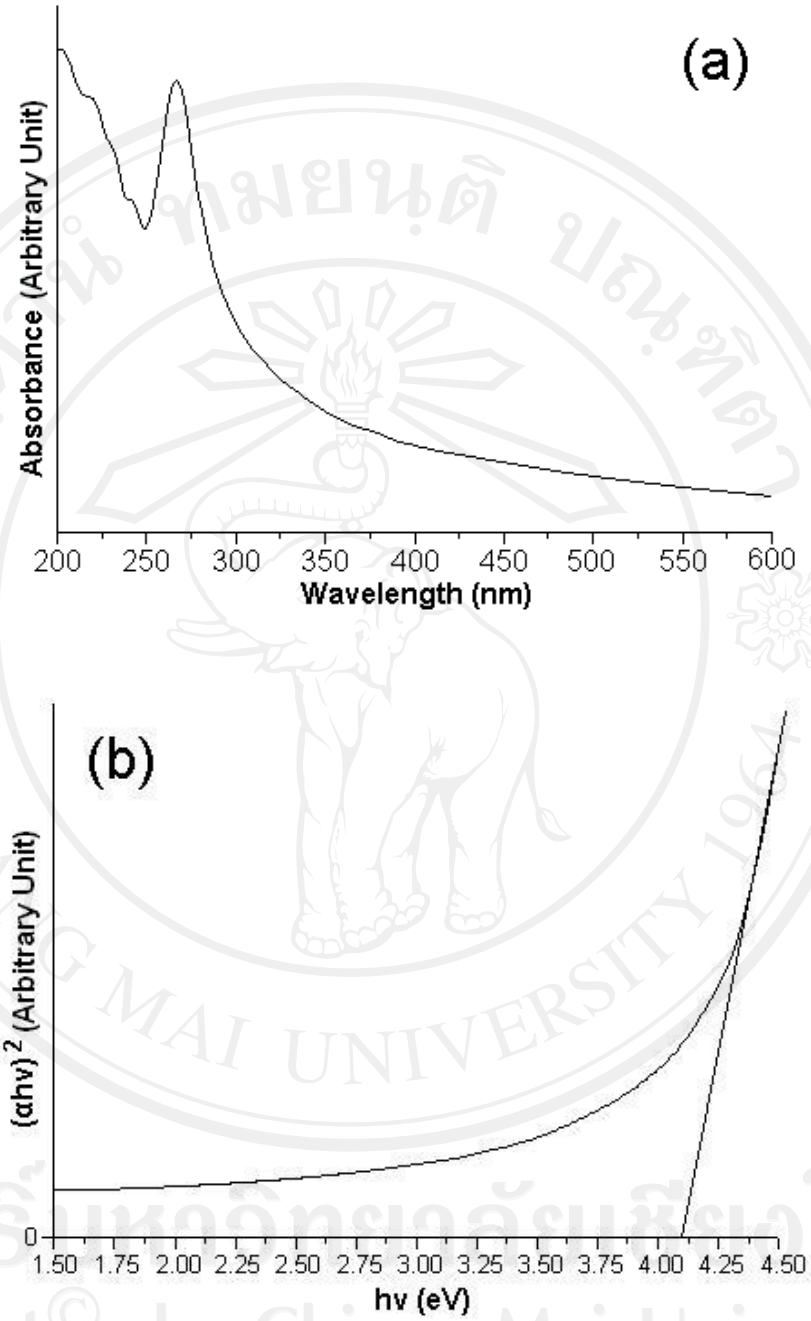

Figure 3.9 (a) UV-visible spectrum, and (b) the plot of $(\alpha h\nu)^2$ versus hν of o-WO_3 microflowers, synthesized by the hydrothermal reaction at 200 °C for 24 h in the solution containing 7.50 ml of 1M HCl.

UV–vis absorbance for o-WO_3 microflowers (Figure 3.9 (a)) shows an absorption band in the 200–450 nm range and a strong band at 275 nm, attributed to the high UV spectrum [42]; this might be a consequence of the confined nature of electrons in the [0 1 0] direction [34]. No absorption band in the visible range was detected. This result is in accordance with those reported by Nataraj and co-workers [25], and Xu and co-workers [42]. The direct band gap (E_g) of o-WO_3 microflowers was determined by Eq.

$$\alpha h\nu = (h\nu - E_g)^n \quad (4)$$

where α, h, ν, and E_g are the absorbance, Planck constant, photon frequency, and optical band gap, respectively. The parameter n is a pure number associated with the different types of electronic transitions: n = 1/2, 2, 3/2 or 3 for direct–allowed, indirect–allowed, direct–forbidden and indirect–forbidden transitions, respectively [43]. Its direct energy gap was determined by extrapolation of the linear portion of the curve (Figure 3.9 (b)) to $\alpha = 0$, corresponding to 4.10 eV.

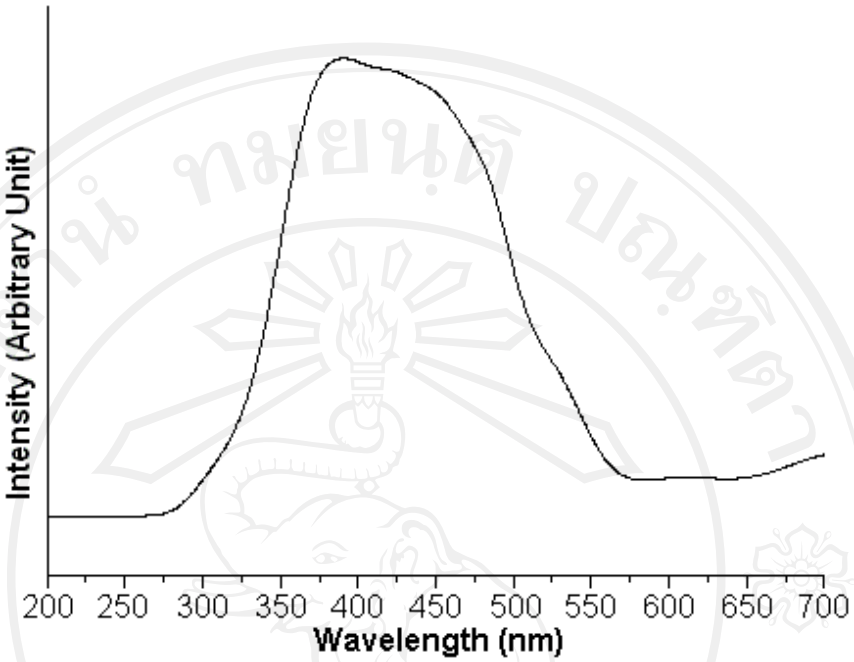

Figure 3.10 PL spectrum of o-WO_3 microflowers.

The PL spectrum (Figure 3.10) of the as-synthesized o-WO_3 microflowers was recorded using 200 nm excitation wavelength at room temperature. The emission peak presents a broad band at 275–575 nm with a maximum emission at 375 nm in the violet region by Gaussian curve fitting, due to the electronic transition of WO_3. This PL emission is in accordance with the report of Lee and co-workers [44].

3. 2 Result of the products synthesized by a hydrothermal method using sodium tungstate dihydrate as a tungsten source

3.2.1 Effect of acidity

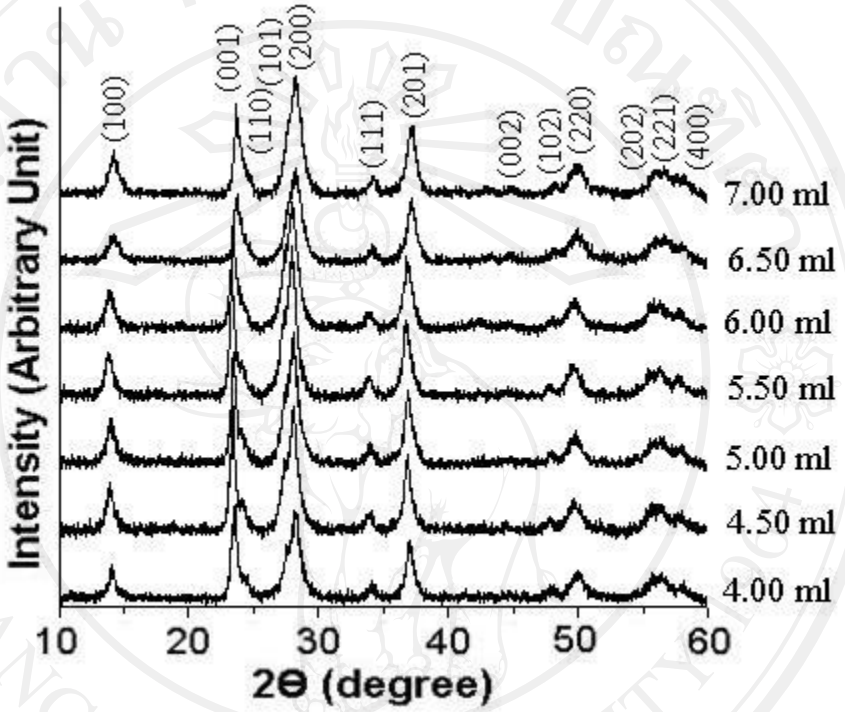

Figure 3.11 XRD patterns of the products synthesized by the hydrothermal reaction at 180 °C for 24 h in the respective solutions containing 4.00 ml, 4.50 ml, 5.00 ml, 5.50 ml, 6.00 ml, 6.50 ml and 7.00 ml of 3M HCl.

Figure 3.11 shows the XRD patterns of the products synthesized by 180 °C, 24 h hydrothermal reactions using sodium tungstate as a tungsten source, with 4.00–7.00 ml 3M HCl added. All diffraction peaks can be indexed and specified that the products crystallized as hexagonal WO_3 (h-WO_3) with no detection of impurities. These patterns were consistent with the literature data (JCPDS file no. 33-1387) [29].

In the 4.00 ml 3M HCl-added solution, the XRD peaks are low intensities. By increased 3M HCl to 4.50, 5.00, 5.50 and 6.00 ml, the XRD peaks became higher in intensities. The strongest intensity peak was at 2θ = 28.1 degrees belonging to the (200) plane of the products. But, the XRD peak became lower intensities in the 6.50 ml 3M HCl-added precursor solution.

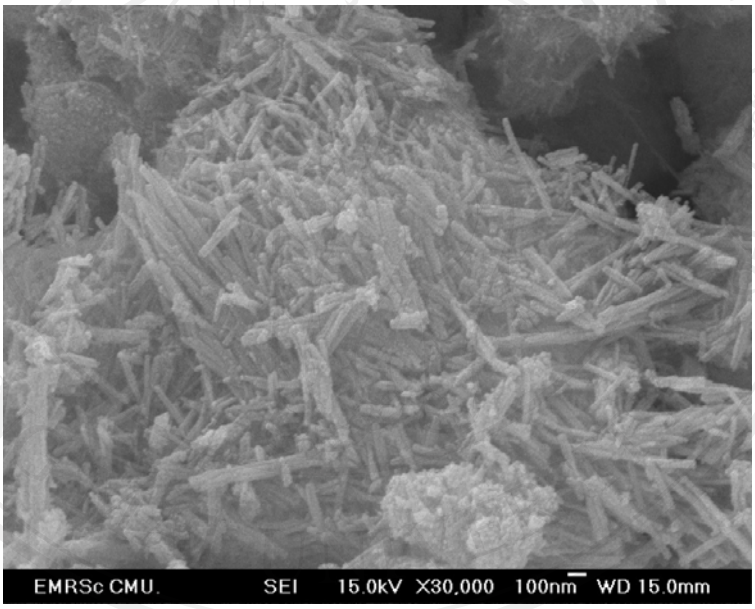

Figure 3.12 SEM image of the product synthesized by the hydrothermal reaction at 180 °C for 24 h in the solution containing 4.00 ml 3M HCl.

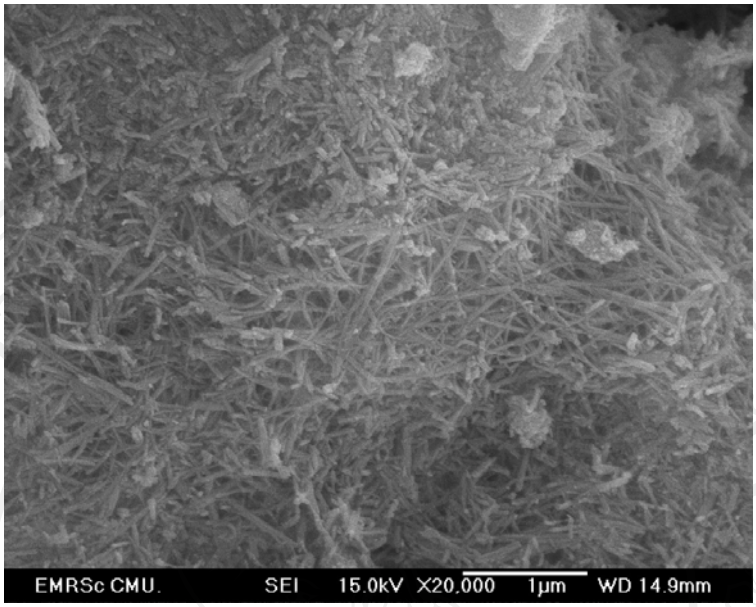

Figure 3.13 SEM image of the product synthesized by the hydrothermal reaction at 180 °C for 24 h in the solution containing 4.50 ml 3M HCl.

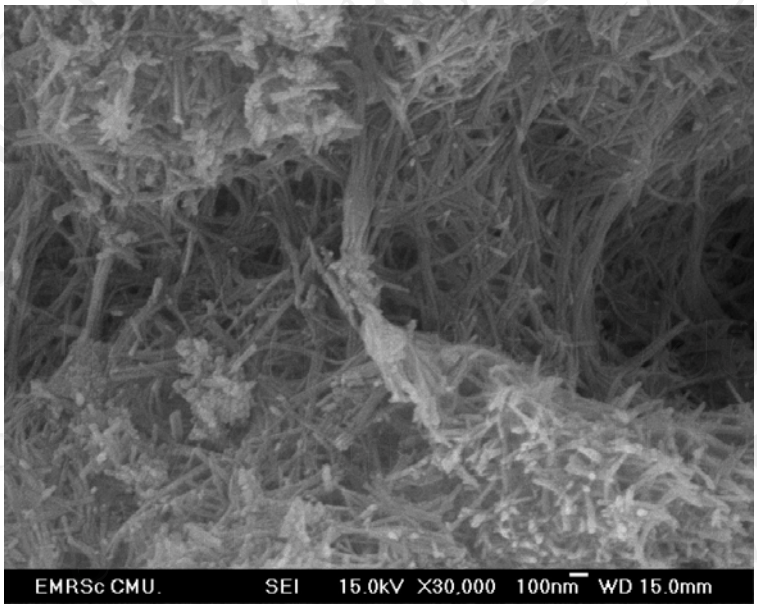

Figure 3.14 SEM image of the product synthesized by the hydrothermal reaction at 180 °C for 24 h in the solution containing 5.00 ml 3M HCl.

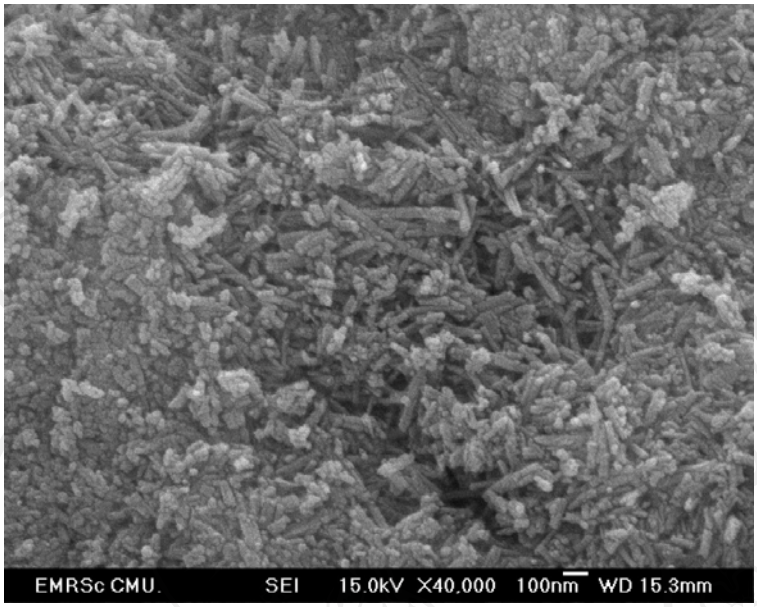

Figure 3.15 SEM image of the product synthesized by the hydrothermal reaction at 180 °C for 24 h in the solution containing 5.50 ml 3M HCl.

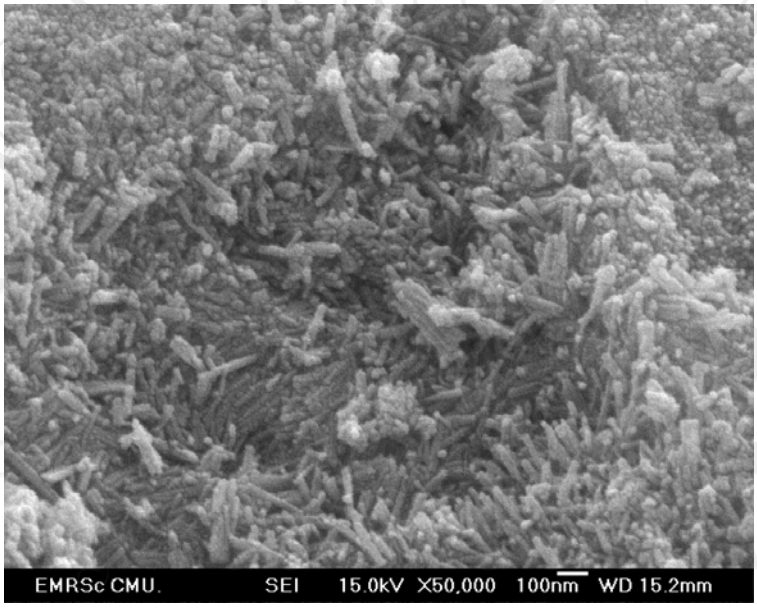

Figure 3.16 SEM image of the product synthesized by the hydrothermal reaction at 180 °C for 24 h in the solution containing 6.00 ml 3M HCl.

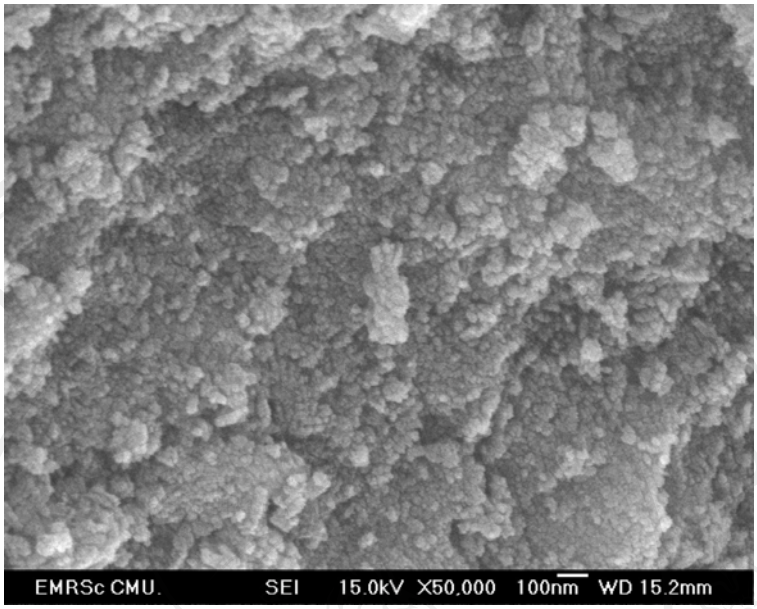

Figure 3.17 SEM image of the product synthesized by the hydrothermal reaction at 180 °C for 24 h in the solution containing 6.50 ml 3M HCl.

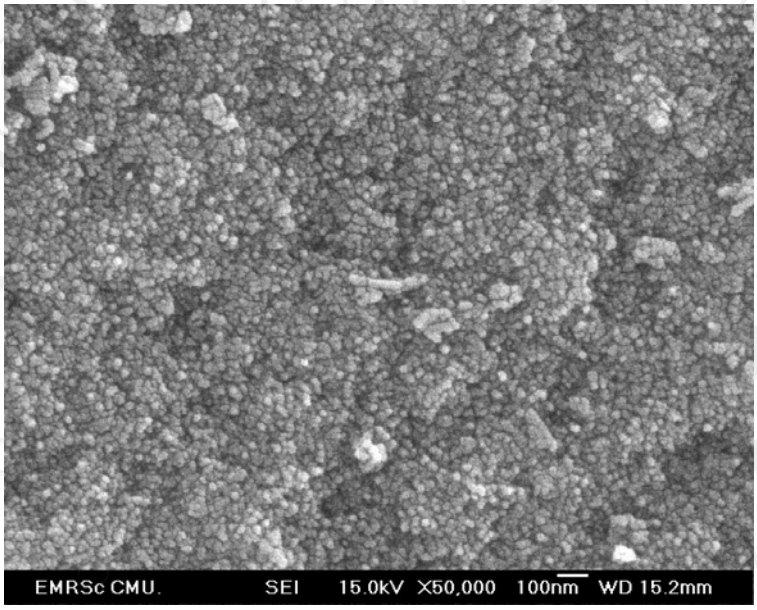

Figure 3.18 SEM image of the product synthesized by the hydrothermal reaction at 180 °C for 24 h in the solution containing 7.00 ml 3M HCl.

SEM images of the products (Figures 3.12-3.18) show the morphologies of those prepared using different volumes of 3M HCl. In the 6.50 and 7.00 ml 3M HCl-added solution, h-WO_3 nanoparticles were produced. When 6.00 ml 3M HCl was added to the solution, a mixture of nanoparticles and nanorods of h-WO_3 was produced. In the 4.00 and 5.50 ml 3M HCl-added solution, h-WO_3 nanorods were produced. The morphologies of h-WO_3 became nanowires in the 4.50 and 5.00 ml 3M HCl-added precursor solutions.

From the XRD pattern and SEM images, the 5.00 ml 3M HCl-added precursor solution was chosen to study the effect of reaction temperature and time.

3.2.2 Effect of reaction temperature

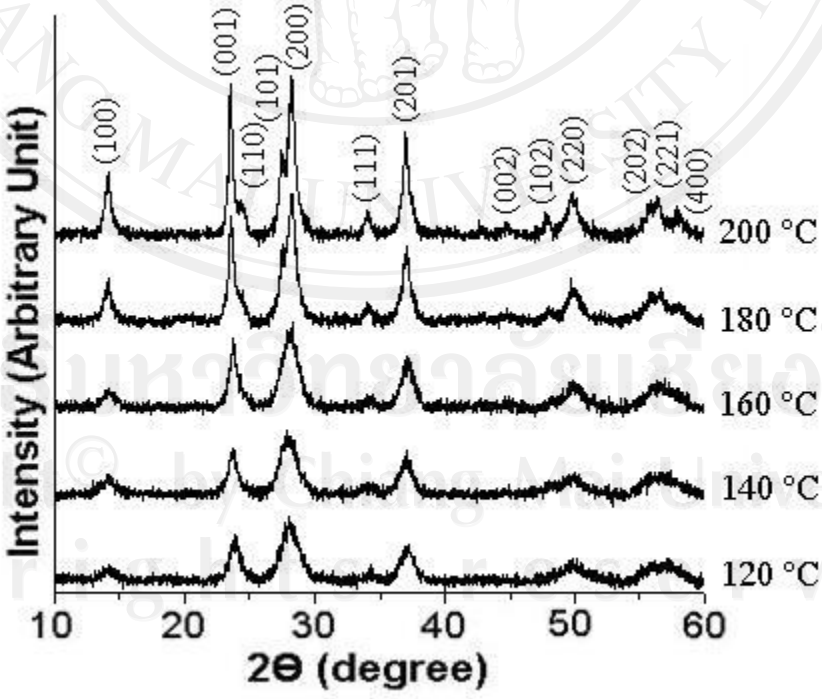

Figure 3.19 XRD patterns of the products synthesized by the hydrothermal reaction at 120, 140, 160, 180 and 200 °C for 12 h in the solution containing 5.00 ml 3M HCl.

Figure 3.19 shows the XRD patterns of the products synthesized by hydrothermal reactions using sodium tungstate as a tungsten source, with 5.00 ml 3M HCl added at different reaction temperatures for 12 h. All diffraction peaks can be indexed and specified that the products crystallized as hexagonal WO_3 (h-WO_3) with no detection of impurities. These patterns were consistent with the literature data (JCPDS file no. 33-1387) [29]. Under hydrothermal reaction at 120 °C for 12 h, the XRD peaks are very broad which show lower crystalline degree with small particles sizes. By increasing the temperature reaction to 200 °C, the XRD peaks became higher in intensities. The strongest intensity peak was at 2θ = 28.2 degrees belonging to the (200) plane of the products. Therefore, hydrothermal reaction at 200 °C was chosen to study the effect of reaction time.

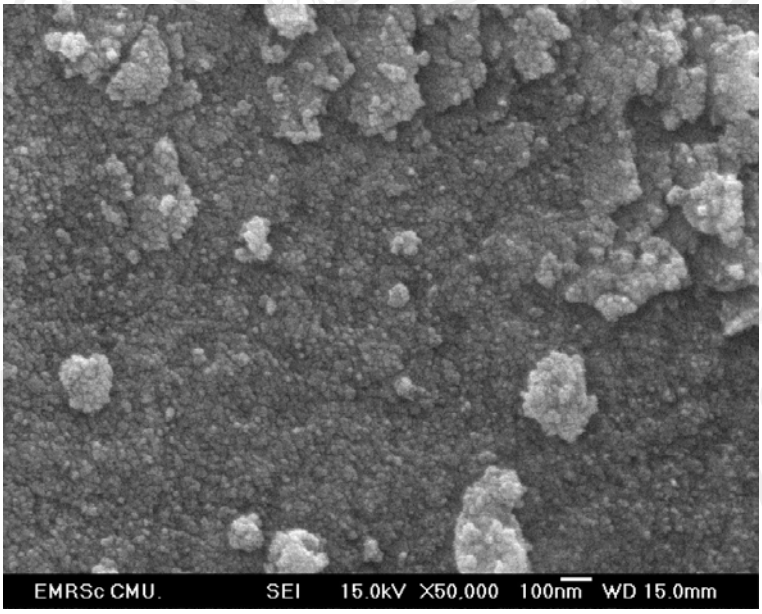

Figure 3.20 SEM image of the product synthesized by the hydrothermal reaction at 120 °C for 12 h in the solution containing 5.00 ml 3M HCl.

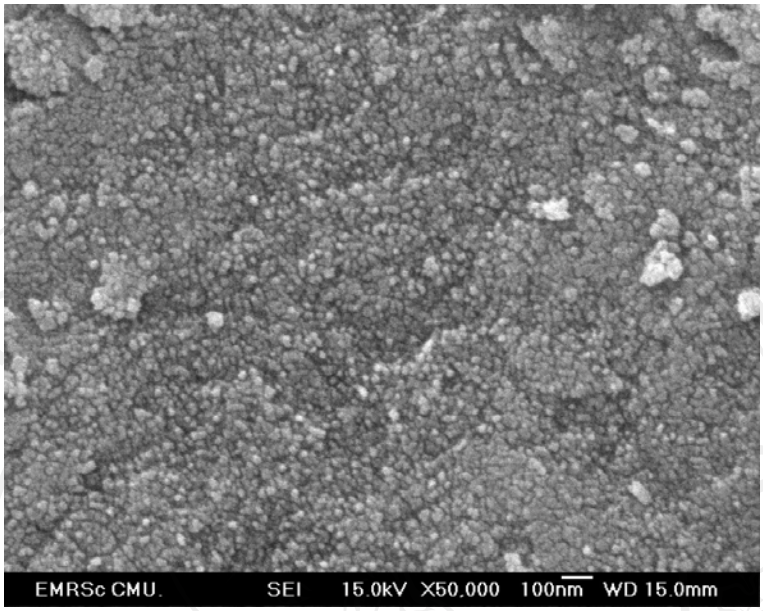

Figure 3.21 SEM image of the product synthesized by the hydrothermal reaction at 140 °C for 12 h in the solution containing 5.00 ml 3M HCl.

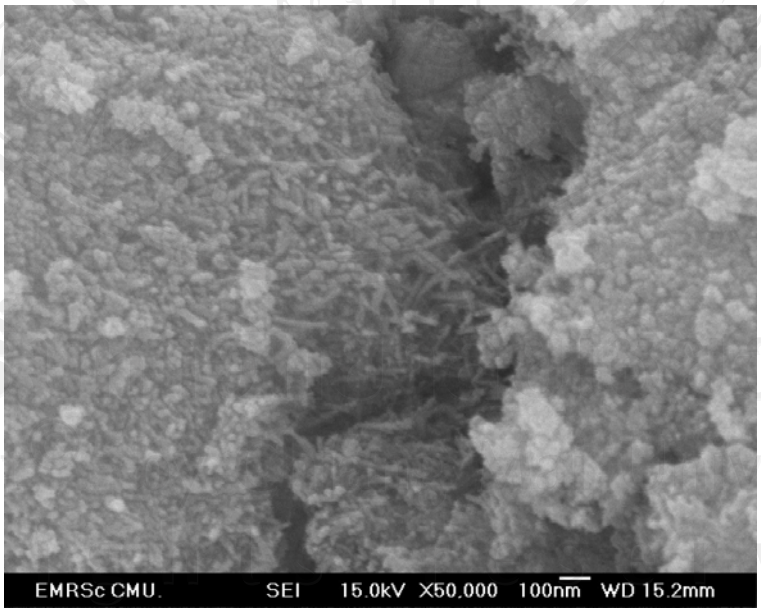

Figure 3.22 SEM image of the product synthesized by the hydrothermal reaction at 160 °C for 12 h in the solution containing 5.00 ml 3M HCl.

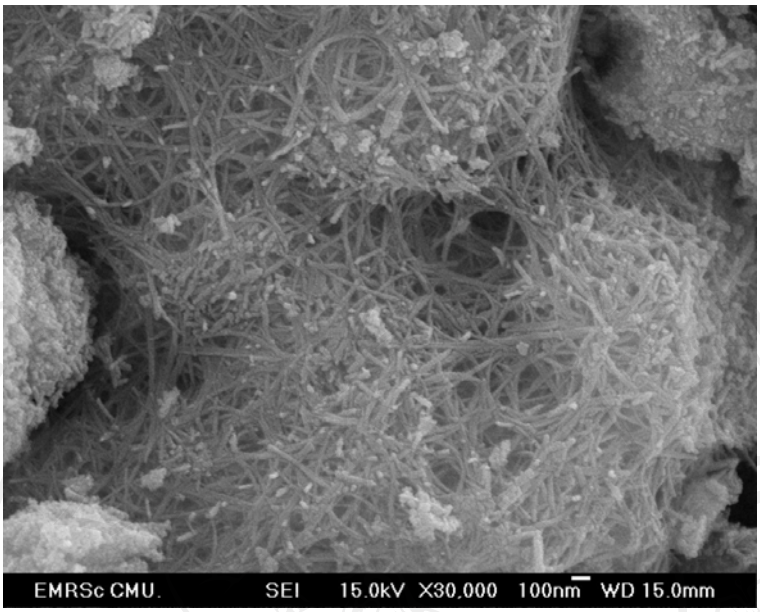

Figure 3.23 SEM image of the product synthesized by the hydrothermal reaction at 180 °C for 12 h in the solution containing 5.00 ml 3M HCl.

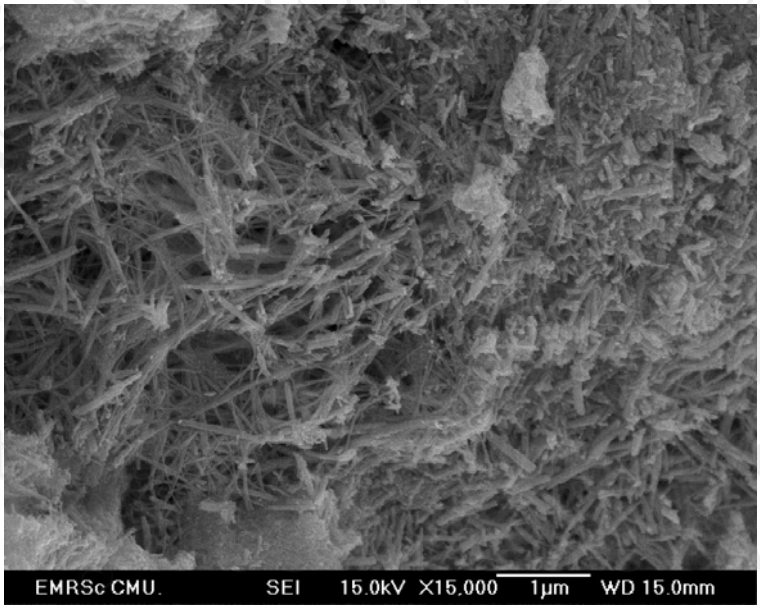

Figure 3.24 SEM image of the product synthesized by the hydrothermal reaction at 200 °C for 12 h in the solution containing 5.00 ml 3M HCl.

SEM images of the products (Figures 3.20-3.24) show the morphologies of the products prepared using 5.00 ml 3M HCl-added solution at different reaction temperatures. The reaction temperatures were 120, 140, 160, 180 and 200 ^{o}C and the reaction time was fixed at 12 h. At 120 and 140 ^{o}C, h-WO_3 nanoparticles were produced. At 160 ^{o}C, h-WO_3 nanorods began to form. By increasing the temperature reaction to 180 and 200 °C, the morphologies of h-WO_3 became nanowires.

3.2.3 Effect of reaction time

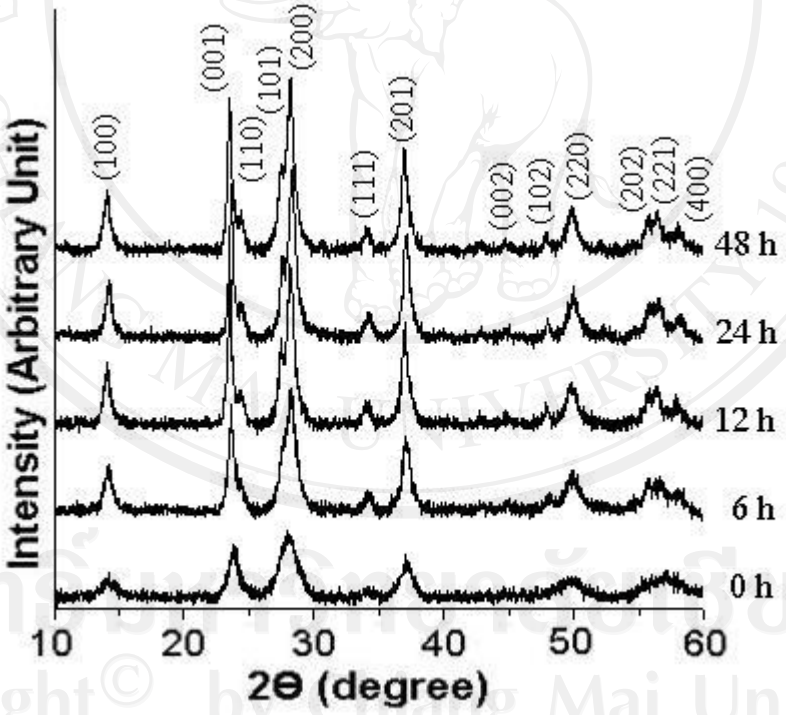

Figure 3.25 XRD patterns of the products synthesized by the hydrothermal reaction at 200 °C for 0, 6, 12, 24 and 48 h in the solution containing 5.00 ml 3M HCl.

Figure 3.25 shows the XRD patterns of the products synthesized by 200 °C hydrothermal reactions at different reaction time using sodium tungstate as a tungsten source, with 5.00 ml 3M HCl added. All diffraction peaks can be indexed and specified that the products crystallized as hexagonal WO_3 (h-WO_3) with no detection of impurities. These patterns were consistent with the literature data (JCPDS file no. 33-1387) [29]. Under hydrothermal reaction at 200 °C for 0 h, the XRD peaks are very broad which show lower crystalline degree with small particles sizes. By increasing the reaction times were lengthen to 48 h, the XRD peaks became higher in intensities. The strongest intensity peak was at 2θ = 28.2 degrees belonging to the (200) plane of the products.

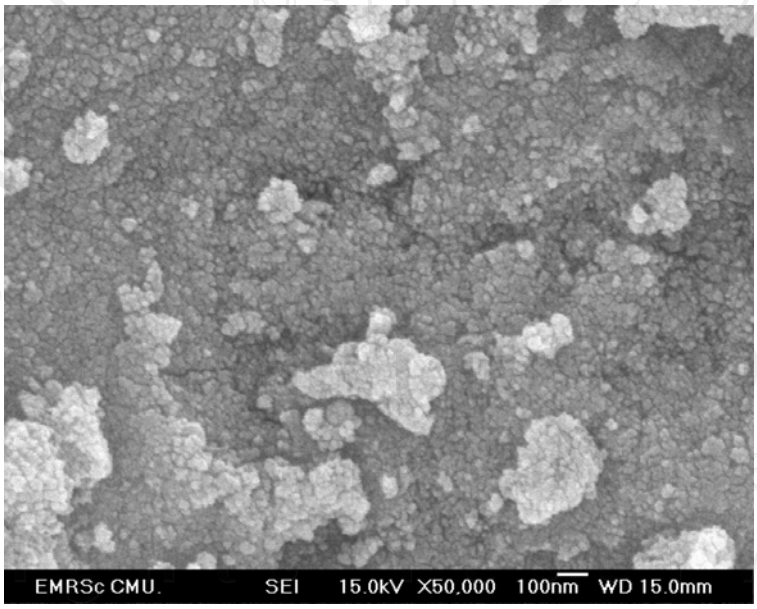

Figure 3.26 SEM image of the product synthesized by the hydrothermal reaction at 200 °C for 0 h in the solution containing 5.00 ml 3M HCl.

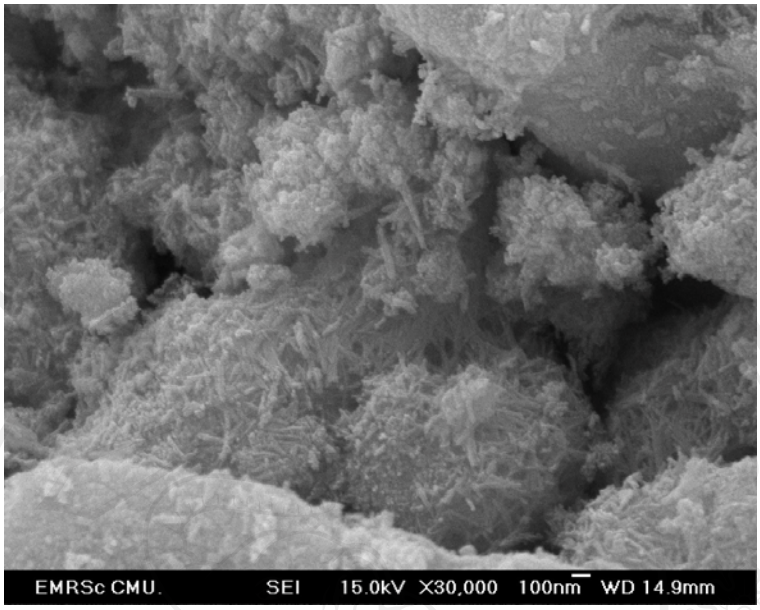

Figure 3.27 SEM image of the product synthesized by the hydrothermal reaction at 200 °C for 6 h in the solution containing 5.00 ml 3M HCl.

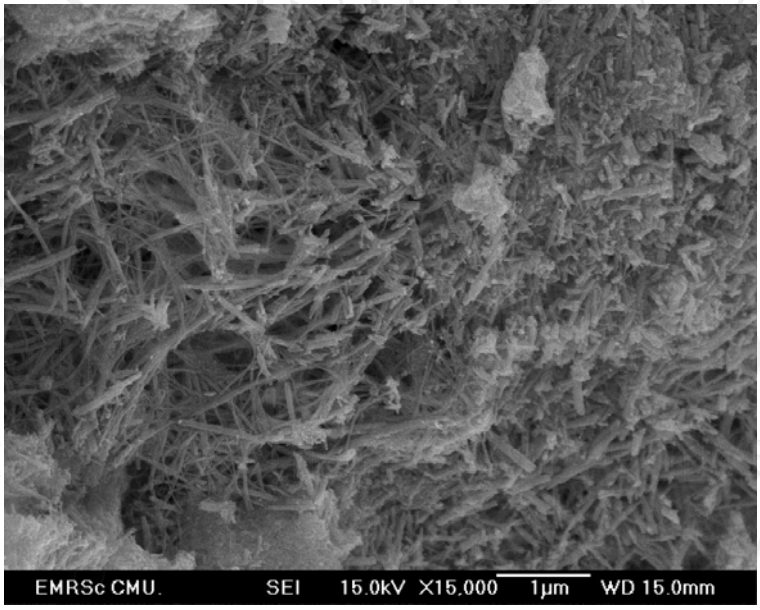

Figure 3.28 SEM image of the product synthesized by the hydrothermal reaction at 200 °C for 12 h in the solution containing 5.00 ml 3M HCl.

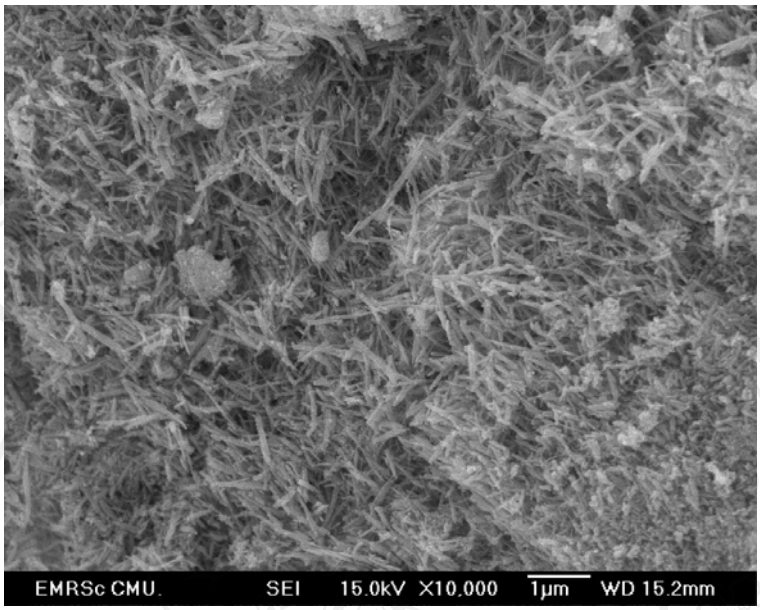

Figure 3.29 SEM image of the product synthesized by the hydrothermal reaction at 200 °C for 24 h in the solution containing 5.00 ml 3M HCl.

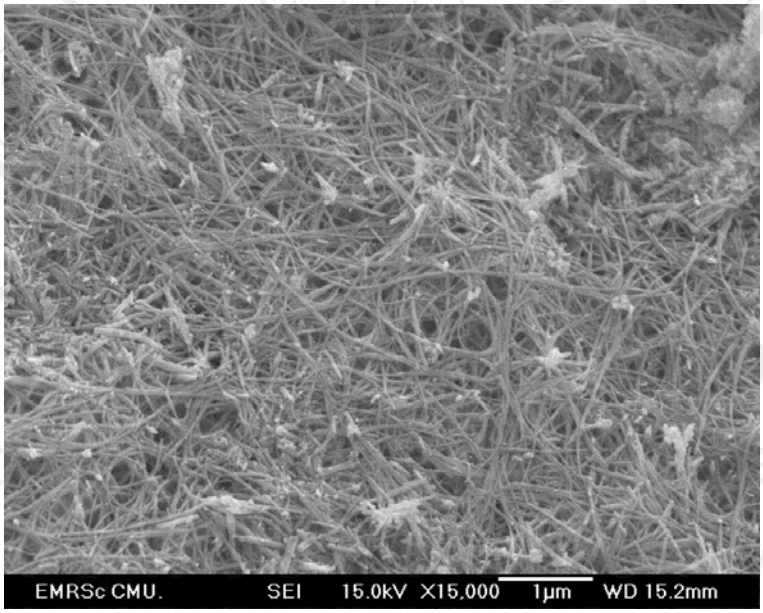

Figure 3.30 SEM image of the product synthesized by the hydrothermal reaction at 200 °C for 48 h in the solution containing 5.00 ml 3M HCl.

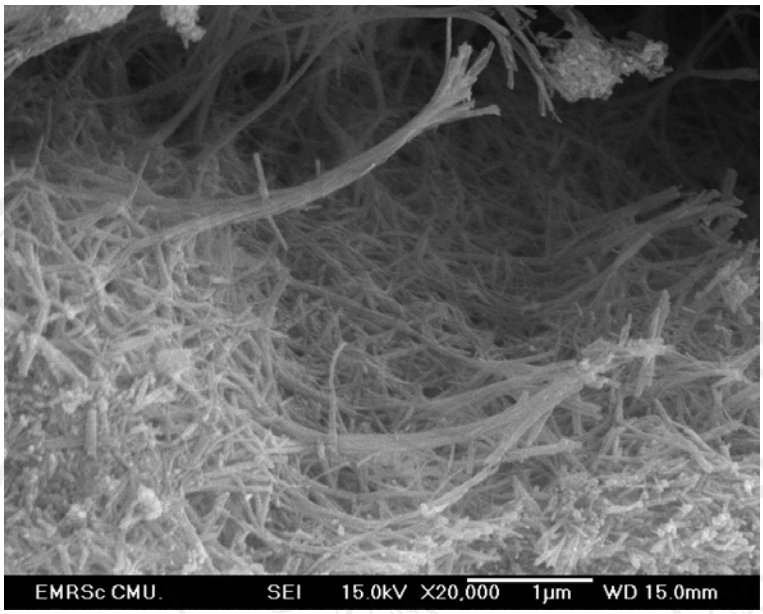

Figure 3.31 SEM image of the product synthesized by the hydrothermal reaction at 200 °C for 72 h in the solution containing 5.00 ml 3M HCl.

SEM images of the samples (Figures 3.26-3.31) show the morphologies of the products prepared using 5.00 ml 3M HCl-added solution synthesized by 200 °C hydrothermal reactions at different reaction time. At 0 h, h-WO_3 nanoparticles were produced. At 6 h, h-WO_3 nanorods began to form, and subsequently grew into nanowires by the 12 and 24 h reaction. At 48 h of the reaction, the complete h-WO_3 nanowires formation took place with diameter of 20-30 nm and length grew to several micrometers. Further prolonging the reaction time up to 72 h, the length of the nanowires only was increased to a small extent.

Thus, optimum reaction temperature and holding time for the highly crystalline h-WO_3 nanowires were determined to be 200 ^oC and 48 h, for the hydrothermal process.

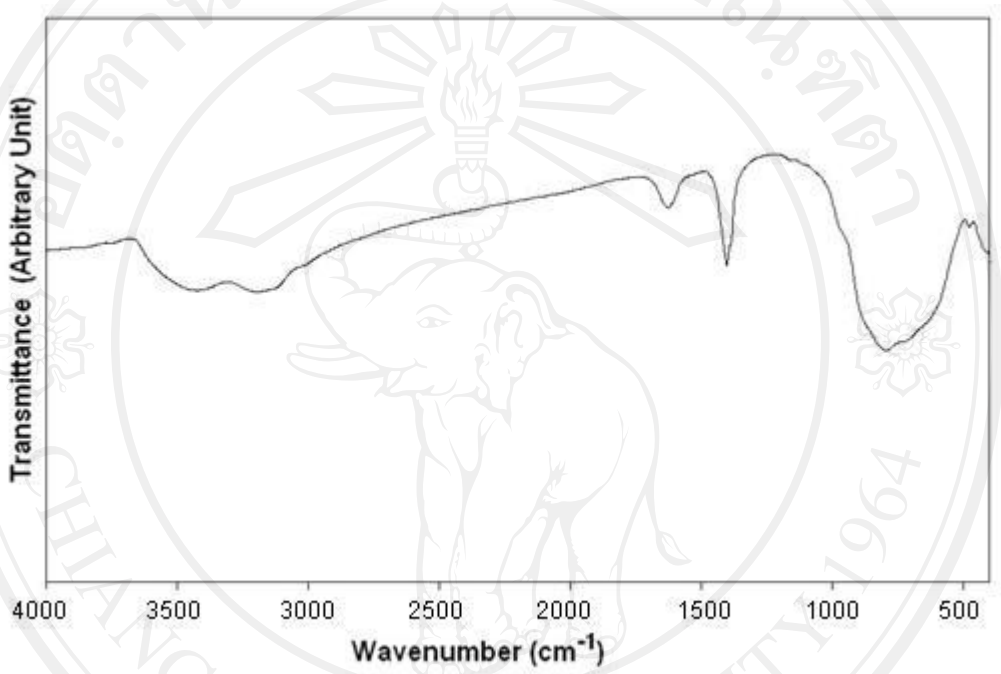

Figure 3.32 FTIR spectrum of product synthesized by the hydrothermal reaction at 200 °C for 48 h in the solution containing 5.00 ml 3M HCl.

FTIR spectrum of h-WO_3 is shown in Figure 3.32. They presented a broad band in the range 2800-3650 cm^{-1}, two sharper peaks located at 1400 and 1632 cm^{-1}, and a broad band in the range 500-1000 cm^{-1}. The broad band in the range of 2800-3650 cm^{-1} and two sharper peaks at 1400 and 1632 cm^{-1} were caused by air contamination - they are at higher sensitive to moisture. The bands at the 2800-3650 cm^{-1} range and a peak at 1632 cm^{-1} are assigned to be ν(OH) and δ(OH) modes of

adsorbed water, respectively. The splitting of the broad band and the presence of 1400 cm^{-1} peak of the earlier studies were specified as unusual values of the stretching ν(OH) and bending δ(OH) vibrations: indicating OH groups had the strong bond to either water molecules or surface oxygen atoms. The band at 3210 cm^{-1} and 1400 cm^{-1} have been assigned to the stretching vibrations of NH_4^+ from starting materials because it was not completely removed by washing with water and ethanol. For the vibration wavelength below 1000 cm^{-1}, the FTIR spectra showed two peaks at 706 and 813 cm^{-1}, assigned as a shortening of the W–O bonds of h-WO_3. All these bands are in good accordance with the report of Phuruangrat *et al.* [2] and Rougier *et al.*[45].

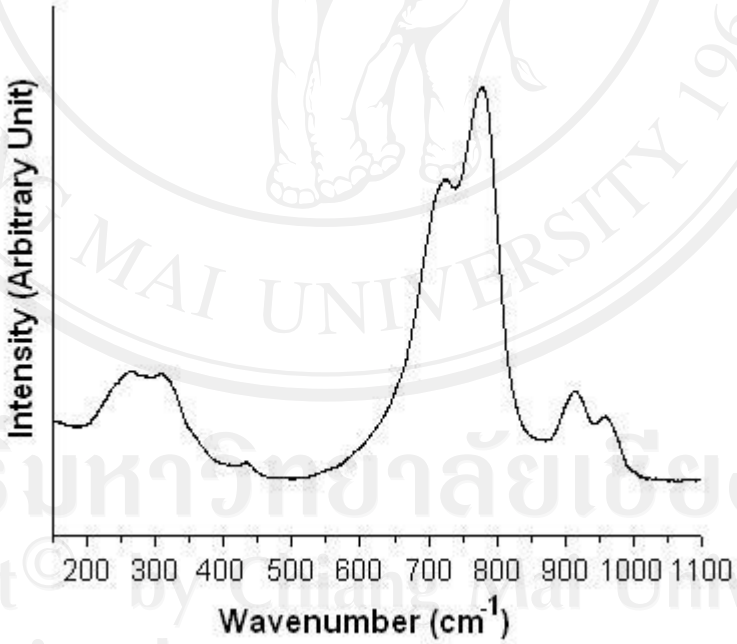

Figure 3.33 Raman spectrum of product synthesized by the hydrothermal reaction at 200 °C for 48 h in the solution containing 5.00 ml 3M HCl.

The Raman spectrum of the as-synthesized WO_3 nanowires over the range of 150–1100 cm^{-1} is shown in Figure 3.32. The most intense peak is centered at 780 cm^{-1} with a shoulder at 730 cm^{-1} and they are attributed to the symmetric and asymmetric vibrations of W^{6+}–O bonds (O–W–O stretching modes). Two peaks centered at 320 and 270 cm^{-1} correspond to W–O–W bending modes of the bridging oxygen. A peak at 910 cm^{-1} with a shoulder positioned at 960 cm^{-1} was also detected, corresponding to the W=O stretching mode of terminal oxygen atoms. The small feature at 435 cm^{-1} is attributed to the characteristic band of crystalline WO_3. All these peaks are in good accordance with the report of Huirache-Acuña and co-workers [10].

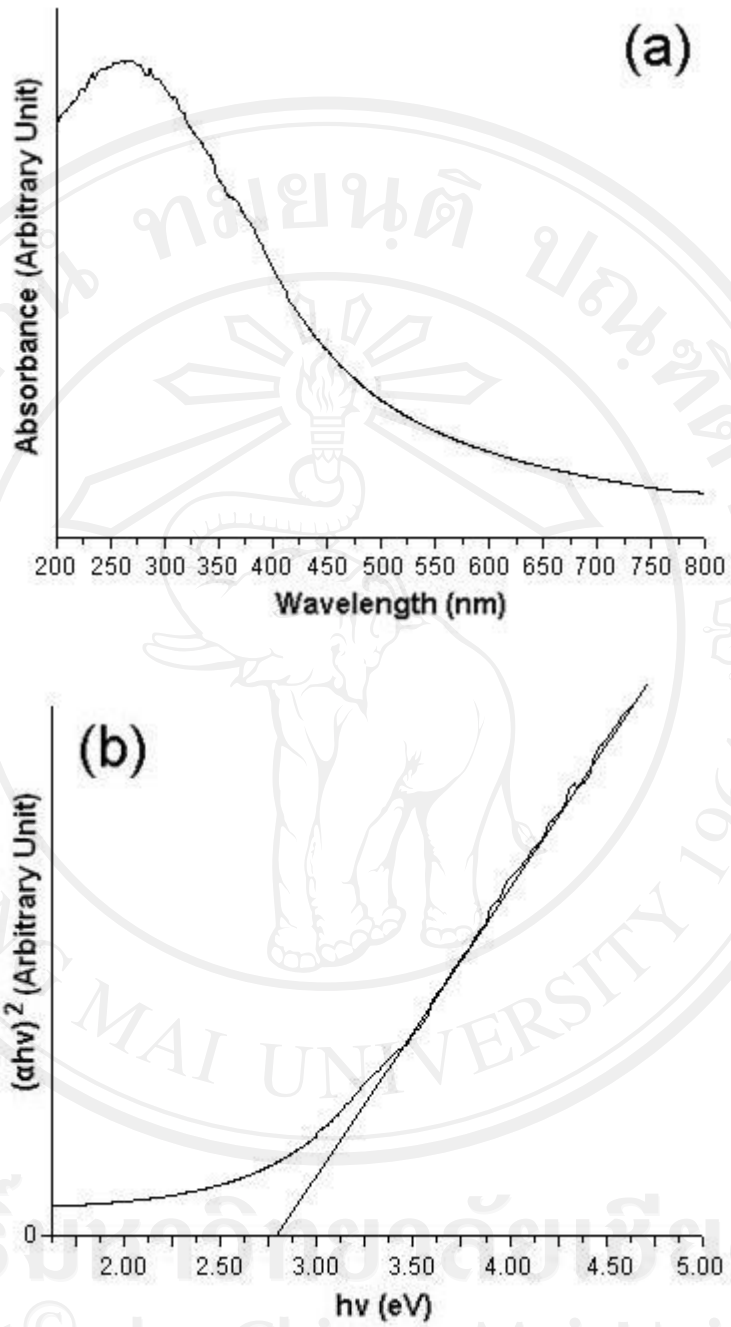

Figure 3.34 (a) UV-visible spectrum, and (b) the plot of $(\alpha h\nu)^2$ versus hν of products synthesized by the hydrothermal reaction at 200 ^{o}C for 24 h in the solution containing 7.50 ml of 1M HCl.

UV–vis absorbance for h-WO_3 nanowires (Figure 3.34 (a)) shows the absorption spectrum with a peak maximum at 275 nm. This result is in accordance with the report of Nataraj and co-workers [25]. The direct band gap (E_g) of h-WO_3 nanowires was determined by Eq. (4). Its direct energy gap was determined by extrapolation of the linear portion of the curve (Figure 3.34 (b)) to $\alpha = 0$, corresponding to 2.80 eV.